Article:
Liao, P., Wang, T., Tang, T.-Q. et al. (2025) Two-Stage Lane-Changing Driving Strategy Based on Driving Habits and Vehicle Dynamics for Autonomous Electric Vehicles. IEEE Transactions on Intelligent Transportation Systems. ISSN: 1524-9050

https://doi.org/10.1109/TITS.2025.3579123

Two-stage lane-changing driving strategy based on driving habits and vehicle dynamics for autonomous electric vehicles

Peng Liao, Tao Wang, Tie-Qiao Tang, Ronghui Liu

***Abstract*—Lane-changing (LC) critically affects traffic efficiency and safety, making it a key focus in autonomous driving strategy development. In the human-machine co-driving phase, assisted driving systems must integrate driver habits to enable effective driver-vehicle collaboration. To this end, this paper proposes an LC strategy for autonomous electric vehicles (EVs) that integrates driver habits and vehicle dynamic characteristics. It solves two crucial issues: (1) how to guarantee drivers' LC habits in the proposed strategy, and (2) how to maximize the utilization of electric vehicle (EV) dynamics on the LC performance. In the lane-changing decision (LCD) stage, we estimate the LC probability to obtain a range of LC starting positions that align with driver habits, and we select one to enhance the EV performance. In addition, in the lane-changing implementation (LCI) stage, we propose an anthropomorphic EV control to ensure the LC trajectory is consistent with driver habits, while the EV dynamics are optimized with different trajectory objectives. The simulation results show the driver's LCD is dependent on the longitudinal position difference between the preceding vehicles in the original and target lanes, and the LCD predicted accuracy reaches 95.2%. In addition, the proposed LCI can meet the differentiated LC demands, as the LCI strategies focusing on economy, comfort, and efficiency can reduce the SOC consumption by 28.6%, the wheel angular velocity by 94.4%, and the LC duration by 70.0%, respectively. Besides, the robustness of the strategy is verified by the relatively stable performance under SOCs and environment temperatures. Thus, this paper has the potential to clarify the LC optimization requirements for autonomous EVs and assist in the electrification and intelligent development of transportation systems.**

***Index Terms*—Lane-changing, driving habits, logit model, electric vehicle dynamics, two-degree-of-freedom vehicle model**

I. Introduction

DURING the driving process, drivers exhibit two typical driving behaviors [1]–[3], namely car-following (CF) and lane-changing (LC). Driver needs to determine the driving behavior to be executed based on the obtained traffic information (e.g., position, velocity, and acceleration). This decision-making is influenced by the driver's driving habits. Following the decision-making process, the driver regulates the vehicle's motion through the operation of the accelerator, brake, and steering wheel to accomplish the intended driving behavior.

Drivers are required to continuously make and execute decisions based on the surrounding environment, placing a significant burden on them. Relevant statistics [4] indicate that 96.2% of traffic accidents result from driver errors, with cognitive errors, decision-making errors, and improper operations accounting for 41%, 33%, and 11%, respectively. Assisted driving can help alleviate driver stress by supporting decision-making and execution, while also enhancing driving safety.

This study focuses on the LC strategy in an assisted driving system. Developing an effective LC strategy for electric vehicles (EVs) in the assisted driving system is challenging. The reasons that lead to the challenges are: (i) Compared to CF, which involves only longitudinal control, LC requires coordinated longitudinal and lateral movements. (ii) The widespread adoption of EVs introduces new challenges to optimizing LC behavior due to electric vehicle (EV) complex dynamics. (iii) It is more important to obtain an LC strategy that is consistent of (at least not deviate excessively from) driver's intent, since the deviation may induce great panic for drivers [5].

Existing research on EV LC has yet to comprehensively harmonize trajectory optimization with driving habit adaptation. From the perspective of trajectory planning, studies typically replicate driver trajectories to develop anthropomorphic strategies, aligning with driver habits but retaining undesirable behaviors. Others optimize LC trajectories for an "optimal path", yet overlook driver expectations, potentially discouraging the use of assisted driving systems. In addition, EV LC strategies must fully account for vehicle dynamics and internal system coordination, particularly the operational characteristics of the battery.

To fill these gaps, this study develops a two-stage LC strategy considering driving habits and EV properties for autonomous vehicles. In the first stage, we develop a driver intention model to ensure that drivers can quickly adapt to the LC strategy of the assisted driving system. In the second stage, we integrate the kinematics and battery characteristics of EVs to enhance the economy, comfort, and safety of the LC trajectory. Specifically, we utilize driver trajectory data and vehicle motion characteristics to construct a logit-based LCD model, reproducing the driver's real-time LC intention accurately. Then, we propose an LCI model to quickly generate the LC trajectory considering the EV operation properties. Finally, we develop the final LC optimization strategy with

This work was supported by the National Natural Science Foundation of China (72288101,72201149), the Natural Foundation of Shandong Province (ZR2024QE314), and the Fundamental Research Funds for the Central Universities (202413022).

P. Liao is with College of Engineering, Ocean University of China, Qingdao, China; T. Wang is with School of Automotive and Transportation Engineering, Hefei University of Technology, Hefei, China; T.Q. Tang is with School of Transportation Science and Engineering, Beihang University, Beijing, China; R. Liu is with Institute for Transport Studies, University of Leeds, Leeds, U.K.

Corresponding author: T. Wang; Email: istaowang@gmail.com

the consolidation between the LCI and LCD models.

The remainder of this paper is organized as follows: Section II presents the literature review. Section III develops the LCD model to align with driver habits. Section IV introduces the LCI model to represent EV dynamics. Section V formulates the LC strategy by integrating the LCD and LCI models. Section VI provides a case study and discussion. Finally, Section VII concludes the paper.

II. Literature review

In recent years, research on EV LC strategies for autonomous driving technology has attracted the attention of scholars in mechanical engineering, systems engineering, management science, behavioral science, computer science, psychology, and transportation science. And, the relevant research involves three parts: LC behavior models, EV dynamics models, and LC strategies for autonomous driving.

A. LC behavior models

The LC behavior is the main lateral movement of the vehicle to obtain a better driving environment or move to the expected destination. As for the LC process, the driver first makes a real-time decision on whether to change lanes based on the obtained traffic information, known as the LCD. Then, the LCI is executed, i.e., once the driver decides to change lanes, he/she starts planning and tracking the LC trajectory by controlling the vehicle's accelerator pedal, brake pedal, and steering wheel. In contrast, once the driver decides not to change lanes, he/she performs CF behavior or travels at the desired velocity. Thus, the LC behavior model exhibits obvious two-stage characteristics, i.e., LCD and LCI.

The LCD model aims to reproduce the driver's decision on the choice between CF and LC, focusing on the expression of the microscopic decision-making behavior and the calibration of physical parameters. The relevant studies mainly include rule-based models, learning-based models, etc. The rule-based model is the most basic framework for modeling LCD, and there is a clear causal relationship between explanatory variables (e.g., relative distance) and dependent variables (e.g., acceleration). The Gipps model [6] is the earliest rule-based LCD model, which summarizes the LCD process as a decision tree with a series of fixed conditions and ultimately outputs a binary choice result, i.e., LC or no LC. After Gipps' groundbreaking work, many scholars have extended and improved this framework. Yang et al. [7] modeled mandatory and discretionary LCD according to purposes and scenarios. Jin et al. [8] proposed an LCD rule considering the longitudinal distance, which poses a simple structure and strong interpretability. Another mainstream LCD model is induced from learning methods. Compared to the rule-based LCD model, adequate data training qualifies the LCD model based on learning methods with stronger generalization ability and higher adaptation to complex situations. Xie et al. [9] proposed a data-driven LC model based on deep learning models to address the complexity and uncertainty of driving behavior. Wang et al. [10] constructed a prediction method based on a fuzzy inference system and a long short-term memory neural network to comprehensively consider the relationship between the driving environments and the drivers. Ali et al. [11] studied an LCD model framework that explains the mandatory and discretionary LC behaviors considering the game theory-based approach.

The interaction between the driver's LCI process and the motion of surrounding vehicles can be revealed by the existing LCI model from the micro level. For the sake of exploring this interaction, as well as the correlation between this interaction and various traffic phenomena, researchers have studied the LCI process based on the theory of motion waves [12]. Laval et al. [13] developed a motion wave hybrid model, in which LCI vehicles are approximated as motion bottlenecks, and each lane is modeled as a separate motion wave flow interrupted by the LCI vehicles. In addition, cellular automata are applied in the LCI to reproduce LC behavior with minimal microscopic description. Das et al. [14] explored the microscopic and macroscopic properties of LC activity using cellular automata.

However, all these LC behavior models are mainly focusing on the accurate reproduction of LC behavior, neglecting the adjustable content in driving behavior, thus unable to satisfy the optimization demands of LC behavior.

B. EV dynamics models

With the continuous advancement of vehicle electrification, EVs are bound to become the main type of vehicles in future transportation systems. The study of their dynamic characteristics, namely the relationship between force and motion, has also received a lot of attention from researchers [15], [16]. From the perspective of motion implementation, the systems related to dynamics mainly include the powertrain and the steering system. The driving force to overcome vehicle driving resistance (e.g., wind resistance, slope resistance, rolling resistance, and acceleration resistance) is provided and decided by the powertrain. The driving force generation and transmission involve chemical-to-electrical energy conversion in the battery, electrical-to-mechanical energy conversion in the motor, torque and speed adjustment in the transmission, and subsequent transfer through other components. The EV's velocity direction is governed by both the steering system and the powertrain. The steering system controls wheel rotation, and in conjunction with the vehicle's velocity, adjusts the direction of motion. Manzetti et al. [17] provided a cradle-to-grave analysis of the emerging technologies in the EV battery, with an assessment of green chemistries as novel green energy sources for the EV and microelectronics portable energy landscape. Dai et al. [18] discussed and differentiated conventional engines (e.g., gasoline and diesel-driven engines) versus electromotor and hybrid engines. Ruan et al. [19] estimated whether transmissions are worthwhile for the customer considering the price/performance relationship of design solutions. Zhang et al. [20] presented a control method to improve the safety performance of the EV steering system, and found that the EV steering system exhibits unstable chaotic behaviors at certain speeds.

These existing studies clarify the relationship between the control variables and EV driving performance (e.g., power,

economy, environmental protection, etc.), while ignoring the limitations of real traffic conditions on EV motion status, thus leading to the decrease in the realization of EV performance in real driving.

C. LC strategies for autonomous driving

Autonomous driving technology has the potential to liberate drivers from driving tasks, greatly improving traffic efficiency and safety [21], [22]. The LC behavior is important to improve traffic performance by replacing it with autonomous driving technology. In manual driving, drivers rely on sensory inputs, such as sight and hearing, to perceive the road environment and make driving decisions based on traffic regulations and personal experience. On the contrary, autonomous vehicles rely on the decision-making layer to generate driving trajectories and then utilize the implementation layer to achieve the driving trajectories transmitted from the decision-making layer. Therefore, the existing research on LC for autonomous vehicles mainly includes trajectory planning corresponding to the decision-making layer and trajectory tracking corresponding to the implementation layer.

The trajectory planning is utilized to generate an optimal driving trajectory with regard to surrounding environment, vehicle motion states, and driving time. The commonly adopted methods for autonomous vehicle trajectory planning mainly include the graph search method, the random sampling method, the parameter curve method, the numerical optimization method, etc [23], [24]. Graph search methods, like Dijkstra and A* algorithms, explore graph structures by retrieving raster grids with obstacle information. They assign costs based on grid states and iteratively search for the optimal path from start to endpoint [25]–[27]. The random sampling method searches a path that satisfies collision avoidance detection by randomly selecting nodes that connect the starting point and the target point [28]. The parameter curve method generates the trajectory by curve-fitting, e.g., bezier curves, polynomial curves, and B-spline curves [29], [30]. These curves possess smooth curvature, controllable shapes, and excellent real-time performance, making them capable of meeting the basic requirements for trajectory tracking. The numerical optimization method designs mathematical programming with different objective functions related to driving safety and comfort for optimal trajectory determination [31], [32].

Trajectory tracking is executed to calculate control variables that enable the vehicle to accurately track the planned trajectory, such as wheel steering angle, acceleration, and braking commands [33], [34]. Based on the different dimensions of vehicle motion, trajectory tracking technology can be divided into longitudinal control and lateral control. Longitudinal control calculates accelerator/brake pedal commands based on the error input of the vehicle's longitudinal velocity, enabling the vehicle to track the desired longitudinal position. In addition, lateral control outputs a reasonable wheel steering angle to enable the vehicle to track the desired lateral position. Trajectory tracking not only ensures the tracking accuracy of the vehicle for the planned trajectory, but also focuses on the comfort and safety of passengers. At present, commonly used methods for trajectory tracking include proportion integration differentiation (PID) control, sliding mode control (SMC), model predictive control (MPC), etc. Chu et al. [35] presented a trajectory planning and tracking framework, which applies an artificial potential to obtain target trajectory and MPC with PID feedback to effectively track planned trajectory. Hwang et al. [36] proposed a hierarchically improved fuzzy dynamical SMC to address the autonomous ground vehicle path-tracking problem.

The above studies on autonomous driving strategies mostly explore trajectory planning and trajectory tracking independently, without synergistically optimizing the driver requirements for trajectory planning and the vehicle motion implementation capabilities for trajectory tracking.

III. LCD MODEL CONSISTENT WITH THE DRIVING HABITS

Drivers have the potential to perform the LCD according to the obtained traffic information, such as the position, the velocity, and the acceleration of themselves and the surrounding vehicles. To describe the complexity and randomness of driver decision-making, we adopt LC trajectory data to analyze the characteristics of LCD and construct the LCD models considering different influencing factors.

A. Data preparation

This study examines drivers' behavioral choices in the road traffic system by analyzing the correlation between vehicle motion data and LCD, leveraging vehicle trajectory data. We employ the Next Generation Simulation (NGSIM) dataset to capture LC characteristics [37], [38]. The NGSIM dataset were collected along a 630m segment of the US-101 highway (Fig. 1), comprising five main lanes (Lanes 1–5) and an auxiliary lane (Lane 6), during the morning peak (7:50–8:35 a.m.) on June 15, 2005.

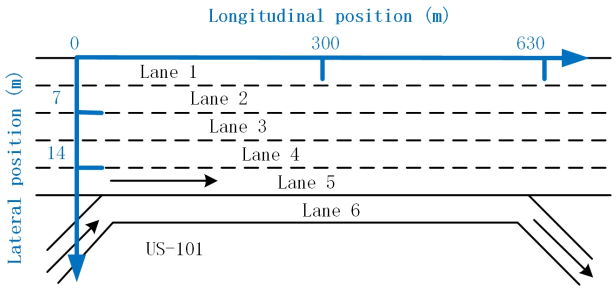

Fig. 1. Schematic coordinate axis diagram of US-101 highway inspection section.

To fully explore the influencing factors on the LCD, we select the dynamics of the six surrounding vehicles as the input data to analyze the EV driver's LCD, as shown in Fig. 2. The dynamics include the longitudinal position, lateral position, speed, and their difference with ego vehicle. m are utilized as the m-th surrounding vehicle of the ego vehicle, where $m \in \{0, 1, 2, 3, 4, 5, 6\}$. $m = 0 \dots 6$ represent the ego vehicle, the front vehicle in the original lane, the rear vehicle in the original lane, the front vehicle in the non-target lane, the rear vehicle in the non-target lane, the front vehicle in the target lane, and the rear vehicle in the target lane, respectively.

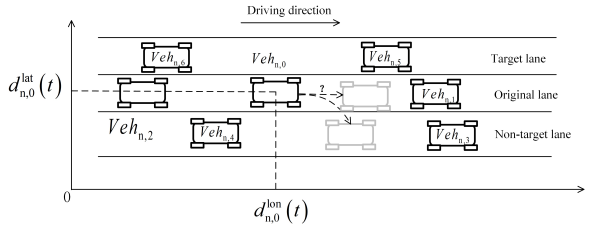

Fig. 2. Movement diagram of the LC vehicle and its surrounding 6 vehicles.

B. Key Points Determination

The drivers in the road traffic system will conduct the LCD based on the current road traffic information (such as position, velocity, and acceleration of their own vehicles, as well as the position, velocity, and acceleration differences with the surrounding vehicles), and then drive the vehicle to complete the corresponding driving tasks. When the driver decides to follow the preceding vehicle, the main task is to maintain a stable following state by adjusting the velocity. In contrast, once the driver decides to perform LC behavior, the main task is to select the appropriate time to drive the vehicle toward the target lane.

Therefore, the LC key points, i.e., lane ID change point, LC start point, and LC end point, can be recognized based on the driving process [39], [40]. Considering the NGSIM dataset, lane ID changes can be directly identified from the dataset. The LC start point is defined as the last point before the vehicle crosses the lane line, where lateral acceleration is zero, and the preceding acceleration direction differs from the LC direction(considering the continuous variation of lateral acceleration). The LC end point is the first point after the vehicle crosses the lane line, where lateral acceleration is again zero, and the subsequent acceleration direction differs from the LC direction(considering the continuous variation of lateral acceleration). Fig. 3 presents the trajectory data of the 12th LC vehicle and its six surrounding vehicles. It is noted that the PV and the FV in this figure are the preceding vehicle and the following vehicle, respectively.

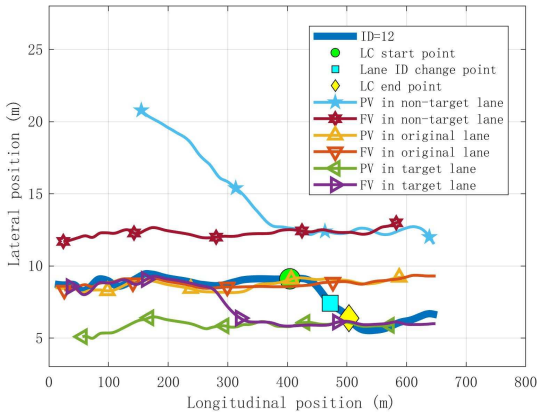

Fig. 3. The trajectory with the LC key points of the 12th LC vehicle and its surrounding 6 vehicles.

C. Statistical properties

To intuitively reflect the driver's differentiation of information, this paper divides the data related to influencing factors into basic information and observation information. The basic information is the longitudinal and lateral position, velocity, and acceleration of the LC vehicle and its surrounding 6 vehicles. The observation information includes the longitudinal and lateral differences of position and velocity between the surrounding 6 vehicles and the LC vehicle.

For a trajectory with LC behavior, we use $\mathtt{p}(t)$ to record whether a vehicle is in the LC process in time slot t, i.e., $\mathtt{p}(t) = \mathbb{1}_{\{t^{\mathrm{lc,s}} \le t \le t^{\mathrm{lc,e}}\}}$, $t^{\mathrm{lc,s}}, t^{\mathrm{lc,e}}$ are the time when a vehicle is at LC starting position and the LC ending position. To calculate the correlation coefficient between influence factors and the LCD, we normalize the dynamics (e.g., velocity, position) of the surrounding vehicles. We use notation $\mathtt{x}$ to represent the generic dynamic of surrounding vehicle. As such, the normalization of the m-th surrounding vehicle's dynamic for vehicle n is formulated as,

$$\mathtt{x}_m^*(t) = \frac{\mathtt{x}_m(t) - \min\left(\mathtt{x}_m(t)\right)}{\max\left(\mathtt{x}_m(t)\right) - \min\left(\mathtt{x}_m(t)\right)} \tag{1}$$

where $\mathtt{x}_m^*(t)$ is the normalized variable of $\mathtt{x}(t)$. With it, we define the correlation coefficient between variable $\mathtt{x}$ with $\mathtt{p}^{\mathrm{LC}}(t)$, as in Eq. (2).

Note that: the subscript "n" denotes the n-th vehicle in the NGSIM data, we omit the subscript in other equations when we do not use the data to analyse the LC process. In addition, the subscript in other equations always denotes the No. of the surrounding vehicle, unless explicitly stated otherwise.

$$\mathtt{cor}_{\mathtt{x},\mathtt{p}} = \sum_{n=1}^{N}\left(\frac{\frac{1}{N}\sum_{i=1}^{N_{n,m}^{\mathrm{LC}}}\left(\mathtt{p}_n(t_i)-\overline{\mathtt{p}_n}\right)\left(\mathtt{x}_{n,m}^*(t_i)-\overline{\mathtt{x}_{n,m}^*}\right)}{\sqrt{\sum_{i=1}^{N_{n,m}^{\mathrm{LC}}}\left(\mathtt{p}_n(t_i)-\overline{\mathtt{p}_n}\right)^2\sum_{i=1}^{N_{n,m}^{\mathrm{LC}}}\left(\mathtt{x}_{n,m}^*(t_i)-\overline{\mathtt{x}_{n,m}^*}\right)^2}}\right) \tag{2}$$

where $\mathtt{cor}_{\mathtt{x},\mathtt{d}}$ is the correlation coefficient between the m-th dynamic variable and the LCD, N is the number of the LC vehicles in NGSIM data, $N_{n,m}$ records the number of time slots of the m-th dynamic of vehicle n, $\overline{\mathtt{x}}$ represents the average value of variable $\mathtt{x}$. The correlation between the surrounding vehicle dynamics with the LCD under the NGSIM data is illustrated in Fig. 4.

The correlation coefficients presented in Fig. 4 highlight the influence of vehicle motion data on LCD. Specifically, the LCD has strong correlations with the longitudinal position and velocity of the ego vehicle and its six surrounding vehicles, as well as with the lateral velocity of the ego vehicle. In addition, some key factors include the longitudinal position difference between the ego vehicle and the front vehicle in the target lane, and the longitudinal velocity difference between the ego vehicle and various vehicles, such as those in the original and target lanes. Consequently, selecting different influential factors from these 28 variables to construct LCD models can provide deeper insights into the driver's LCD behavior.

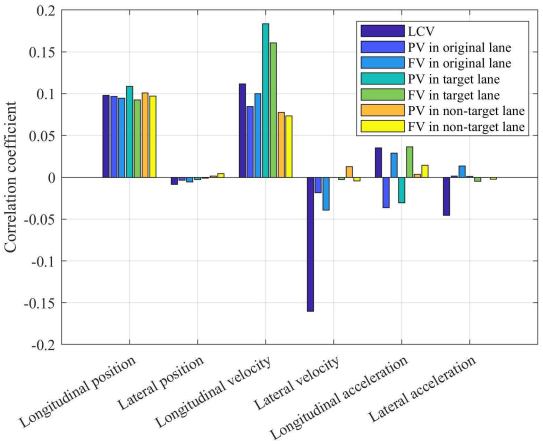

(a)

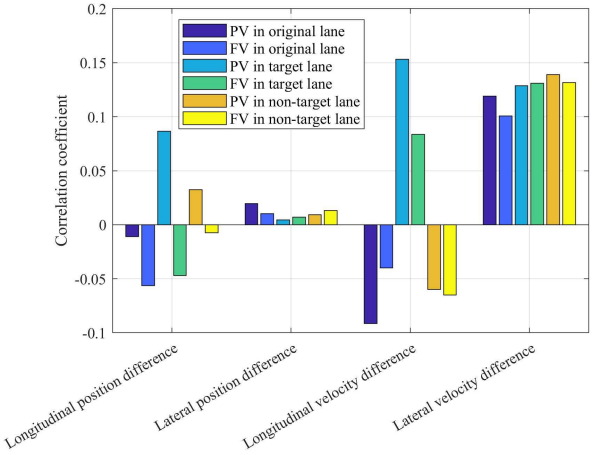

(b)

Fig. 4. Correlation coefficient between information and LCD variables. (a) basic dynamics; (b) relative dynamics.

D. Logistic choice model

The LCD variable is a typical 0-1 variable, so this paper utilizes the logistic regression model to reproduce the driver's LCD. To explore the predictive accuracy of proposed models considering different factors, this paper constructs logistic LCD models considering different influencing factors according to the correlation coefficient magnitude [41].

$$\mathrm{L}^r(t) = \frac{e^{\gamma_0+\gamma_1 x_1(t)+\cdots+\gamma_r x_r(t)}}{1+e^{\gamma_0+\gamma_1 x_1(t)+\cdots+\gamma_r x_r(t)}} \tag{3}$$

where $\mathrm{L}^r(t)$ is the predictive LCD calculated by the Log-it choice model with r factors vehicle; $x_r(t)$ is the value of the r-th dynamic variable at time t; γ_r is the corresponding coefficient of the r-th dynamic variable. We utilize least squares method to calibrate the model parameters, the coefficients in the Log-it model with 28 factors is concluded in Tab. I. We also use a 4-factors and 2-factors models to predict the LCD, the coefficients are recorded in Tab. II and Tab. III.

Since the LCD variable is binary, the accuracy of the LCD model is defined as the average proportion of predicted values before the initiation of LC that are lower than those at the start of LC for each vehicle, as illustrated in Fig. 5. The accuracy

TABLE I
CALIBRATION COEFFICIENT OF LCD MODEL WITH 28 FACTORS

Factor	Value	Factor	Value	Factor	Value
d_0^{lon}	0.00	v_3^{lon}	-1.10	Δv_5^{lon}	0.00
d_1^{lon}	-13.01	v_4^{lon}	-0.73	Δv_6^{lon}	0.00
d_2^{lon}	0.00	v_5^{lon}	6.43	Δv_1^{lat}	-1.41
d_3^{lon}	-2.64	v_6^{lon}	1.39	Δv_2^{lat}	-1.61
d_4^{lon}	-2.15	v_0^{lat}	-4.31	Δv_3^{lat}	1.92
d_5^{lon}	16.40	Δd_2^{lon}	0.45	Δv_4^{lat}	0.92
d_6^{lon}	2.01	Δd_5^{lon}	-2.36	Δv_5^{lat}	1.86
v_0^{lon}	-2.82	Δv_1^{lon}	-2.98	Δv_6^{lat}	0.96
v_1^{lon}	0.00	Δv_3^{lon}	0.00	γ_0	2.14
v_2^{lon}	-1.43	Δv_4^{lon}	0.00		

Note: the superscript "lat" represents the "Lateral"; "lon" represents the "Longitudinal"; d is vehicle's position; v is vehicle's velocity; Δ means the difference of a variable between the surrounding vehicle and the ego vehicle.

TABLE II
CALIBRATION COEFFICIENT OF LCD MODEL WITH 4 FACTORS

Factor	Value	Factor	Value	Factor	Value
d_1^{lon}	-6.57	v_5^{lon}	2.26	γ_0	2.14
d_5^{lon}	7.13	v_0^{lat}	-6.97		

TABLE III
CALIBRATION COEFFICIENT OF LCD MODEL WITH 2 FACTORS

Factor	Value	Factor	Value	Factor	Value
d_1^{lon}	-5.29	d_5^{lon}	6.21	γ_0	-0.25

of LCD models considering 28 or 4 factors does not differ significantly. However, when only 2 factors are considered, the accuracy increases by 30.41% and 31.31%, respectively. This suggests that reducing the number of factors improves the accuracy of the LCD model, likely because including more factors increases the model's sensitivity to vehicle movements, resulting in missed LC opportunities. The accuracy in recognizing the LC opportunities is indeed improved as the number of factors increases. But this is not consistent with the driver's habits, as the driver's executed LCD requires an obvious LC opportunity to prompt. Therefore, the LCD model considers more factors poses high precision to LC opportunities that meet the driver's expectations, as well as the missed LC opportunity before the driver performs the LC behavior, thus leading to the inconsistency with the driver's driving habit. In order to reproduce the driver's driving habits and ensure the acceptance of the proposed strategy, the predicted value of the ideal LCD model will reach its maximum value at the actual LC starting point executed by drivers. And, the detailed analysis is discussed in "VI. CASE STUDY AND DISCUSSION". This finding indicates that drivers in a traffic system primarily decide to change lanes based on the longitudinal position difference between the lead vehicles in their current and target lanes.

Through the correlation analysis between motion information and LCD, the proposed model considers 2, 4, and 28 influencing factors, respectively, among which the situation of 28 influencing factors has complexity and overfitting. How-

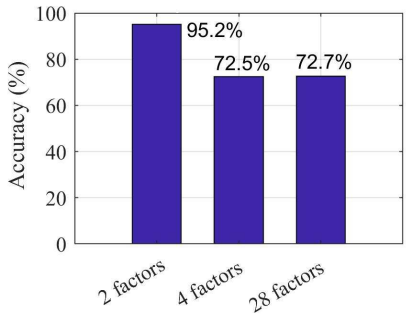

Fig. 5. Prediction accuracy of logistic-based LCD model considering 2, 4, and 28 factors

ever, in the construction of the strategy, to ensure consistency between LCD and driving habits, this paper adopts a LCD model that considers 2 influencing factors, thereby avoiding the complexity of multi-factor coupling and the overfitting effect. It is worth noting that through the replacement and iteration of the dataset, the factors considered will change, but the model constructed according to the new factors will still adapt to the new dataset.

IV. LCI MODEL ACCOUNTING FOR THE ELECTRIC VEHICLE DYNAMICS

The driver's control over the EV during the LC process is reflected in real-time longitudinal and lateral displacement changes. To clarify the quantitative relationships among acting forces, motion state, energy consumption, and control variables, this paper proposes an LCI model based on the dynamic characteristics of EVs, focusing on the powertrain and steering systems.

A. Displacement analysis considering EV dynamics

The quantitative analysis of EV dynamics is a complex multi-factor coupling problem, characterized by the interaction among people, vehicles, roads, and environments. In the driving process, the EV longitudinal and lateral displacement changes are achieved by the driver's operations on the accelerator pedal, the brake pedal, and the steering wheel.

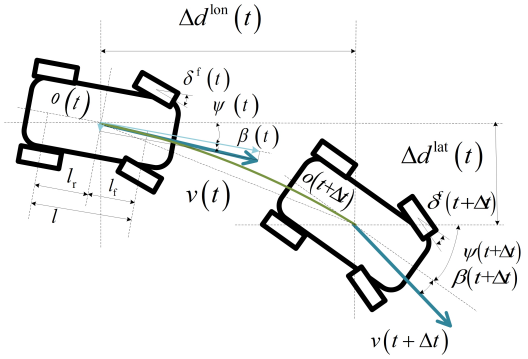

Fig. 6. Vehicle motion based on a two-degree-of-freedom vehicle model

As illustrated in Fig. 6, by fully considering the effects of driver operations on EV velocity, acceleration, and steering angle, a 2-degree-of-freedom vehicle model [42], [43] is employed to describe the relationship between these operations and the real-time EV motion state, as defined by Eqs.(4),(5) and (6).

$$\frac{d\beta(t)}{dt} = C_1^{\beta}\beta(t) + C_2^{\beta}\omega(t) + C_3^{\beta}\delta^f(t) \tag{4a}$$

$$\frac{d\omega(t)}{dt} = C_1^{\omega}\beta(t) + C_2^{\omega}\omega(t) + C_3^{\omega}\delta^f(t) \tag{4b}$$

$$v^{\text{lon}}(t) = v(t)\cos(\psi(t) + \beta(t)) \tag{4c}$$

$$a^{\text{lon}}(t) = a(t)\cos(\psi(t) + \beta(t)) \tag{4d}$$

Eq. (4a) formulate the dynamic of vehicle's sideslip angle β; Eq. (4b) is the dynamic of vehicle's yaw velocity ω, where $\delta^f(t)$ is the front wheel steering angle; in Eq. (4c) and Eq. (4d), $\psi(t)$ is EV yaw angle. Note that, the coefficients are given by,

$$C_1^{\omega} = \frac{k_f l_f^2 + k_r l_r^2}{I_z v^{\text{lon}}(t)} \tag{5a}$$

$$C_2^{\omega} = \frac{k_f l_f^2 + k_r l_r^2}{I_z v^{\text{lon}}(t)} \tag{5b}$$

$$C_3^{\omega} = -\frac{k_f l_f}{I_z} \tag{5c}$$

$$C_1^{\beta} = \frac{k_f + k_r}{M v^{\text{lon}}(t)} \tag{5d}$$

$$C_2^{\beta} = \frac{k_f I_f + k_r I_r}{M v^{\text{lon}}(t)^2} - 1 \tag{5e}$$

$$C_3^{\beta} = -\frac{k_f}{M v^{\text{lon}}(t)} \tag{5f}$$

The parameters in Eq. (5) is concluded in Tab. IV.

TABLE IV
THE PARAMETER MEANINGS IN EQUATION (5)

Notations	Means
k_f	The front wheel equivalent lateral stiffness
k_r	The rear wheel equivalent lateral stiffness
M	The EV mass
l_f	The distance from the EV mass center to the front axle
l_r	The distance from the EV mass center to the rear axle
I_z	The inertia moment of EV revolves around the vertical axis

With the above formulation, notations, and parameters, we formulate the real-time longitudinal and lateral displacement changes, as

$$\begin{aligned}\Delta d^{\text{lon}}(t) = {} & \frac{2 \cdot v^{\text{lon}}(t)}{\omega(t)} \sin\left(\frac{\omega(t)\Delta t}{2}\right) \\ & \times \cos\left(\frac{\omega(t)\Delta t}{2} + \beta(t) + \psi(t)\right)\end{aligned} \tag{6a}$$

$$\begin{aligned}\Delta d^{\text{lat}}(t) = {} & \frac{2 \cdot v^{\text{lon}}(t)}{\omega(t)} \sin\left(\frac{\omega(t)\Delta t}{2}\right) \\ & \times \sin\left(\frac{\omega(t)\Delta t}{2} + \beta(t) + \psi(t)\right)\end{aligned} \tag{6b}$$

where Δt is the time step; $\Delta d^{\text{lat}}(t)$ is the vehicle lateral displacement changes between the time t and time $t+\Delta t$; $\Delta d^{\text{lon}}(t)$ is the vehicle longitudinal displacement changes between the time t and time $t+\Delta t$.

B. Implementation effect of powertrain and steering system

The EV's powertrain and the steering system are crucial for achieving specific acceleration and steering angles. To achieve a particular acceleration, the driving force transmitted from the powertrain to the wheels must counterbalance the driving resistances, including rolling resistance, slope resistance, air resistance, acceleration resistance, and braking force (see Fig. 7).

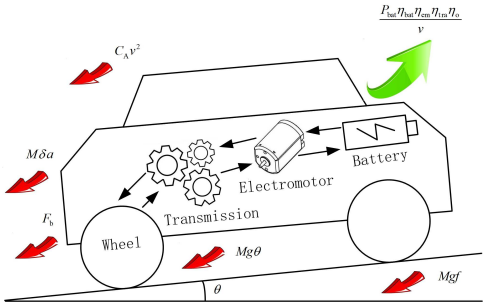

Fig. 7. EV Energy transmission process and acting force

The EV's rotational mechanical energy is generated by the battery and the electromotor. The battery first converts chemical energy into electrical energy, which is then transmitted to the electromotor. The electromotor converts this electrical energy into rotational mechanical energy, which is subsequently transmitted to the transmission or other devices to adjust torque and speed. In addition, EVs recover braking energy during deceleration, with the energy transmission process occurring in reverse. The relationship among acceleration, velocity, forces, and the EV powertrain state is described by Eq. (7) [16], [44]. Similarly, changes in the steering wheel angle, resulting from the driver's operation through the steering system, can be described by Eq. (8).

$$\frac{P_{\text{bat}}\eta_{\text{bat}}\eta_{\text{em}}\eta_{\text{tra}}\eta_o}{v} = Mgf + Mg\theta + C_A v^2 + M\delta a + F_b \quad (7)$$

where P_{bat} is the battery power; η_{bat} is the battery efficiency; η_{em} is the electromotor efficiency; η_{tra} is the transmission efficiency; η_o is the other devices efficiency; M is the EV mass; g is the gravitational acceleration; f is the rolling resistance coefficient; θ is the road slope; C_A is the air resistance coefficient; δ is the acceleration coefficient; F_b is the braking force, and it is directly determined by the driver's operation on the braking pedal.

$$\delta^f = k_{sw}\delta^w \quad (8)$$

where k_{sw} is the proportional coefficient of the steering system; δ^w is the steering wheel angle.

Adequate energy is essential for the powertrain and steering system to achieve the desired EV motion state. However, due to the significant difference in energy requirements for steering and acceleration, the energy cost of the steering system is neglected in this paper. Consequently, the operating states of the battery, electromotor, and transmission are determined using Eqs. (9),(10) and (11), respectively.

$$P_{\text{bat}} = UI \quad (9a)$$

$$U = f_U\left(ET, SOC\right) \quad (9b)$$

$$SOC(t+\Delta t) = SOC(t) - \frac{I(t)\Delta t}{C_{\text{bat}}} \quad (9c)$$

$$\eta_{\text{bat}} = \begin{cases} \frac{P_{\text{bat}} - I^2 r_{\text{dis}}}{P_{\text{bat}}}, & \text{if } a \geq 0 \\ \frac{P_{\text{bat}}}{P_{\text{bat}} + I^2 r_{\text{cha}}}, & \text{otherwise} \end{cases} \quad (9d)$$

$$r_{\text{dis}} = f_{r,\text{dis}}\left(ET, SOC\right) \quad (9e)$$

$$r_{\text{cha}} = f_{r,\text{cha}}\left(ET, SOC\right) \quad (9f)$$

where U is the battery voltage; I is the battery current, and it is directly determined by the driver's operation on the accelerator pedal; ET is the environment temperature; SOC is the battery state of charge; C_{bat} is the battery capacity; r_{dis} is the battery discharge internal resistance; r_{cha} is the battery charge internal resistance; f_U, $f_{r,\text{dis}}$, and $f_{r,\text{cha}}$ are the functions of battery voltage, battery discharge internal resistance, and battery charge internal resistance, respectively. It is noted that these 3 functions are calibrated by the load characteristic experiment, and can be obtained by Ref. [45]–[47].

$$\eta_{\text{em}} = f_{\text{em}}(n_{\text{em}}, T_{\text{em}}) \quad (10a)$$

$$n_{\text{em}} = \frac{30 i_{\text{tra}} i_o v}{\pi r_{\text{whe}}} \quad (10b)$$

$$v(t+\Delta t) = v(t) + a(t)\Delta t \quad (10c)$$

where n_{em} is the electromotor speed; T_{em} is the electromotor torque; i_{tra} is the transmission speed ratio; i_o is the other device speed ratio; r_{whe} is the wheel radius; f_{em} is the function of electromotor efficiency calibrated by the load characteristic experiment, and can be obtained by Ref. [47], [48].

$$\eta_{\text{tra}} = f_{\text{tra}}(i_{\text{tra}}, T_{\text{em}}) \quad (11)$$

where f_{tra} is the function of transmission efficiency calibrated by the load characteristic experiment, and can be obtained by Ref. [49], [50]. It is noted that the adopted transmission is the continuously variable transmission (CVT).

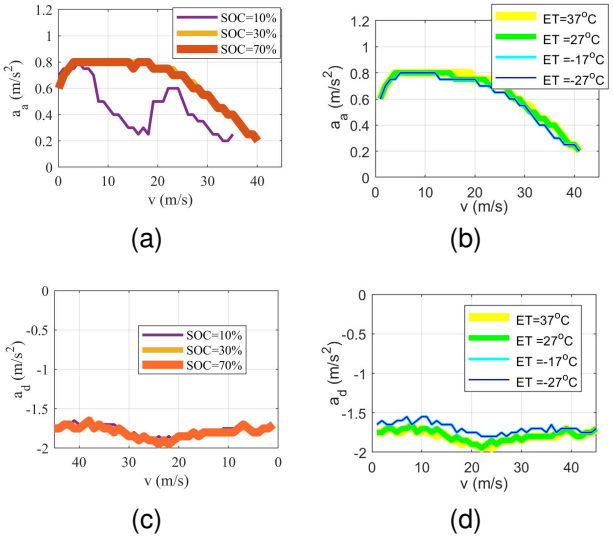

Fig. 8. Adopted acceleration functions in the acceleration stage and the deceleration stage.(a) Acceleration under SOCs; (b) Acceleration under ETs; (c) Deceleration under SOCs; (d) Deceleration under ETs.

C. Trajectory generation based on the LCI

Vehicle trajectory generation is a time-continuous dynamic problem. The trajectory contains the real-time acceleration and steering angle. To address this real-time optimization, this paper proposes a modified form of acceleration and steering angle based on LCI.

EV acceleration is influenced by the driver's pedal operations and powertrain variables. Considering driving habits, the acceleration pattern can be simplified to "acceleration-uniform motion-deceleration". In order to verify the consistency between the proposed velocity variation form and driving habits, this paper selects the LC trajectory of the dataset, with a driver reaction time of 0.5s as the time window, allowing for a 10% velocity fluctuation, to obtain the pattern changes of acceleration, deceleration, and uniform speed, as shown in the Fig. 9. From the perspective of all vehicles, the time proportion of this mode is 66.49% ; From the perspective of a single vehicle, the number of vehicles with a proportion of more than 50% and 80% of the time occupied by this mode is as high as 69.2% and 61.7%, respectively. To optimize the powertrain's operating characteristics and improve computational efficiency, the acceleration value is pre-calculated based on current velocity. Consequently, the real-time acceleration control shifts from determining control variables for the powertrain to managing the duration of acceleration, uniform motion, and deceleration phases. The acceleration can then be determined as

$$a(t) = a_a(v(t)) \cdot \mathbb{1}_{\{t<t_{a,e}\}} + a_d(v(t)) \cdot \mathbb{1}_{\{t_{u,e}<t\leq t_{d,e}\}} \quad (12)$$

where $t_{a,e}, t_{u,e}, t_{d,e}$ are the ending times of the acceleration process, uniform process and deceleration process.The value of $a_a(v(t))$ and $a_d(v(t))$ can be derived and calculated with vehicle powertrain and steering system (Eqs. (4), (7), (8), (9), (10)), by solving the following optimization problems.

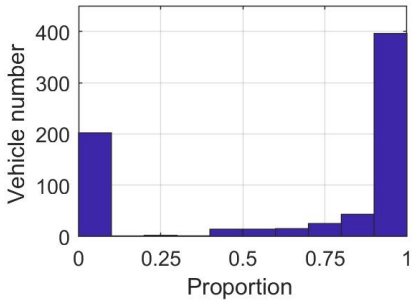

Fig. 9. Distribution of the number of vehicles with velocity patterns.

And, a numerical result for the functions of $a_a(v)$ and $a_d(v)$ is shown in Fig. 8, with the EV parameters in the Ref. [47].

$$a_a(v) = \arg \max_{0\leq a\leq a_{\max}} (\eta_{\text{bat}}\eta_{\text{em}}\eta_{\text{tra}}) \quad (13a)$$

$$a_d(v) = \arg \max_{a_{\min}\leq a<0} (\eta_{\text{bat}}\eta_{\text{em}}\eta_{\text{tra}}) \quad (13b)$$

In the two-degree-of-freedom vehicle model, the wheel steering angle is a key input variable directly controlled by the driver through the steering wheel, with its value being proportional to the steering wheel angle. Considering the driver's specific steering actions, this paper simplifies its variation pattern as "0-increase-constant-decrease-constant-increase-0", where the angular velocity remains constant and each stage has the same duration. To verify the consistency between the proposed angle change form and driving habits, similar to the verification of the velocity change form, this paper selects the LC trajectory of the dataset, takes a driver reaction time of 0.5s as the time window, allows 10% angular velocity fluctuation, and obtains the pattern changes of 0, increase, constant speed, and decrease, as shown in the Fig. 10. From the perspective of all vehicles, the time proportion of this mode is 69.56%; From the perspective of a single vehicle, the number of vehicles with a proportion of more than 50% and 80% of the time occupied by this mode is as high as 79.1% and 37.6%, respectively. Consequently, determining the front wheel steering angle in real-time is reduced to calculating the angular velocity, the duration of angle increase, the duration of constant angle, and the duration of angle decrease. The calculation of the front wheel steering angle is then as follows:

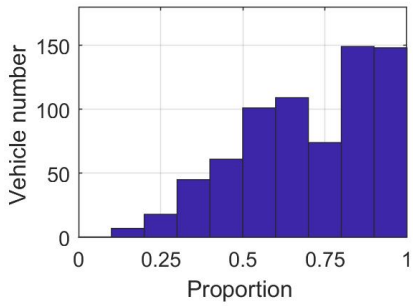

Fig. 10. Distribution of the number of vehicles with angle patterns.

$$\frac{d\delta^f(t)}{dt}=\begin{cases}k^\delta, & t<t_{\text{ang},a,1}\\ 0, & t_{\text{ang},a,1}\le t<t_{\text{ang},u,1}\\ -k^\delta, & t_{\text{ang},u,1}\le t<t_{\text{ang},d}\\ 0, & t_{\text{ang},d}\le t<t_{\text{ang},u,2}\\ k^\delta, & t_{\text{ang},u,2}\le t<t_{\text{ang},a,2}\end{cases} \tag{14}$$

where k^δ is the angular velocity; $t_{\text{ang},a,1}$ is the start time of the 1st angle acceleration stage; $t_{\text{ang},u,1}$ is the start time of the 1st angle unchanged stage; $t_{\text{ang},d}$ is the start time of the angle deceleration stage; $t_{\text{ang},u,2}$ is the start time of the 2nd angle unchanged stage; $t_{\text{ang},a,2}$ is the start time of the 2nd angle acceleration stage. And the start time of each stage should satisfy the constraints induced from the preceding assumptions, i.e.,

$$\begin{cases}t_{\text{ang},a,1}=t_{\text{ang},a,2}-t_{\text{ang},u,2}\\ t_{\text{ang},u,1}-t_{\text{ang},a,1}=t_{\text{ang},u,2}-t_{\text{ang},d}\\ \delta^f\left(t_{\text{ang},a,2}\right)=0\end{cases} \tag{15}$$

V. LC STRATEGY

A. Strategy framework

To achieve optimal driving outcomes, drivers integrate their driving habits with real-time traffic information, including their own vehicle's movement and the movements of surrounding vehicles, to form behavioral intentions such as CF or LC. When traffic conditions meet the criteria for a lane change, the driver forms an LC intention and looks for suitable opportunities to execute the LC by manipulating the accelerator, brake, and steering wheel. It is important to note that the LC implementation is a real-time feedback process, where the autonomous EVs continuously perceive changes in the EV states and adjust operations based on the degree to which the desired driving outcome has been achieved.

Thus, the LC process can be understood as a hierarchical structure, consisting of LCD and LCI. Given the adaptability of driving habits to complex traffic conditions and the limitations of EV dynamics during LC, this paper proposes a layered EV driving strategy that optimizes both the LC initiation point in the LCD stage and the control variables in the LCI stage. The strategy framework is illustrated schematically in Fig. 11.

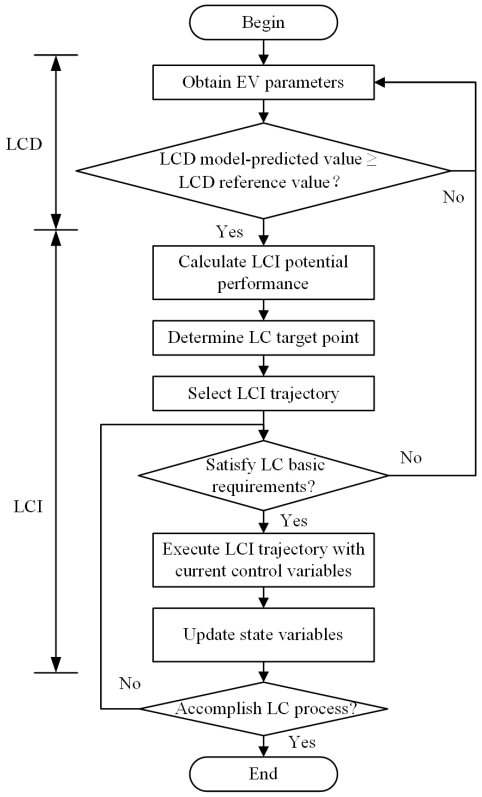

Fig. 11. The Schematic diagram of the strategy framework

B. Optimization of LCD

LCD optimization is employed to replicate the driver's decision-making process in choosing between LC or CF, ensuring alignment between the proposed strategy and typical driving habits. Although drivers adapt to specific and complex traffic situations by choosing LC or CF based on their habits, they often make sub-optimal decisions during execution due to limited rationality and unclear perception of vehicle movement. Therefore, instead of immediately executing LCI, this paper uses the LCD model to determine the optimal LC starting point, serving as the trigger for the proposed strategy.

The Logit-based LCD model, which considers two factors, is utilized due to its high prediction accuracy of 95.2%, effectively capturing the characteristics of driver LC intentions.

$$L^2(i,j)=\frac{e^{-0.25-5.29d_i^{\text{lon}}+6.21d_j^{\text{lon}}}}{1+e^{-0.25-5.29d_i^{\text{lon}}+6.21d_j^{\text{lon}}}} \tag{16}$$

where i,j are the i-th and j-th surrounding vehicles of ego vehicle. Based on the above model, this paper designates the adjacent lanes as target lanes to calculate the real-time LCD values for both. The triggering conditions for the proposed strategy can then be defined as follows:

$$\begin{aligned}L^*=&\mathbb{1}_{\{(L^2(1,5)>L^c)\wedge(L^2(1,3)<L^c)\}}\\ &-\mathbb{1}_{\{(L^2(1,5)<L^c)\wedge(L^2(1,3)>L^c)\}}\end{aligned} \tag{17}$$

where $L^c=\frac{\sum_{m=1}^{N_0^{\text{lc}}}\mathrm{L}^2\left(t_m^{\text{lc,s}}\right)}{N_0^{\text{lc}}}$ is a critical value which denotes the lane changing intention preference. In the formulation of L^c, N_0^{lc} is the number of recorded LC processes of the ego vehicle, $t_m^{\text{lc,s}}$ is the m-th LC starting time for ego vehicle.

C. Optimization of LCI

LCI optimization focuses on determining the optimal LC starting point and EV control variables that achieve desired LC performance metrics, such as consistency, economy, comfort, and efficiency. It is important to note that variations in LC start time alter the EV's motion state, impacting the available space and time for LC, and consequently affecting overall LC performance.

The objective function of the LCI process is Eq. (18), where this paper considered the consistency, economy, comfort, and efficiency of the LC process. Consistency is measured by the

absolute distance difference between the intended LC point and the actual LC start point. Economy is assessed by the change in SOC per unit of longitudinal distance. Comfort is evaluated using the angular velocity of the front wheel, which closely relates to the EV's motion stability. Efficiency is indicated by the LC duration time. Based on these criteria, we should optimize the objective function as follows:

$$\min \xi_{\text{con}} \left| d_0^{\text{lon}}(t_0^{\text{dec}}) - d_0^{\text{lon,s}} \right| + \xi_{\text{eco}} \frac{\Delta \text{SOC}}{\Delta d_{\text{lon}}} + \xi_{\text{com}} k^{\delta} + \xi_{\text{eff}} \Delta T^{\text{lc}} \tag{18}$$

where t_0^{dec} is the time when the LC EV triggering LCD value is not 0; $d_{n,0}^{\text{lon,s}}$ is the LC start longitudinal place of the LC EV; ΔSOC is the SOC change during the LC process; Δd_{lon} is the longitudinal distance change during the LC process; ΔT^{LC} is the duration of the LC process; ξ_{con} is the consistency coefficient with driving habits; ξ_{eco} is the economy coefficient; ξ_{com} is the comfort coefficient; ξ_{eff} is the efficiency coefficient.

Next, we outline the constraints related to LCI optimization. Based on the analysis of LCD and LCI, we explore various LC start points and variables related to acceleration and steering, such as acceleration duration, uniform speed duration, deceleration duration, angular velocity, angle increase duration, constant angle duration, and angle decrease duration. These variables are used to generate multiple LC trajectories with different LCD values, energy consumption rates, wheel angular velocities, and LC times. The optimal LCI trajectory is then selected according to the objective function.

We reduce the feasible solution region with the following constraints.

$$\begin{cases} d_{1,0}^{\text{lc,lon}} \geq d_{n,0}^{\text{lc,lon,s}} + C \\ t^{\text{lc,max}} \geq t_{v,a} + t_{v,u} + t_{v,d} \\ t^{\text{lc,max}} \geq t_{\text{ang},a,1} + t_{\text{ang},u,1} + t_{\text{ang},d} + t_{\text{ang},u,2} + t_{\text{ang},a,2} \\ k^{\delta,\text{max}} \geq \left| k^{\delta} \right| \end{cases} \tag{19}$$

where C is an integrated parameter such that $C = l_f + l_r + 2r_{\text{whe}}$; $t^{\text{lc,max}}$ is the maximum LC time; $k^{\delta,\text{max}}$ is the maximum angular velocity.

Considering the safe operation of the powertrain and steering system, corresponding safety constraints need to be introduced, i.e.,

$$\begin{cases} v_{n,0}^{\min} \leq v_0 \leq v_0^{\max} \\ \delta^{f,\min} \leq \delta^{f} \leq \delta^{f,\max} \end{cases} \tag{20}$$

where $v_{n,0}^{\text{lc,min}}$ and $v_{n,0}^{\text{lc,max}}$ are the minimum and maximum LC EV velocity, respectively; $\delta^{f,\text{min}}$ and $\delta^{f,\text{max}}$ are the minimum and maximum front wheel steering angle, respectively.

To ensure that the LC trajectory aligns with the driver's habits and fully utilizes the vehicle's performance, this paper introduces constraints on the change forms of acceleration and front wheel steering angle in the LCI, as defined in Eqs. (12) and (14). In addition, by incorporating the pre-solved acceleration and deceleration processes (as shown in Fig. 8), these constraints significantly reduce the complexity of solving the optimization problem.

The constraints related to the LCI's end are derived from the LC objectives. The EV not only achieve the desired headway relative to the front vehicle in the target lane but also match its longitudinal velocity and reach the desired lateral velocity. Additionally, the equation assumes the EV is changing lanes to the left, the constraints for the end of the LC are as follows:

$$\begin{cases} d_5^{\text{lon}}\left(t_0^{\text{e}}\right) = d_0^{\text{lon}}\left(t_0\right) + l_f + l_r + 2r_{\text{whe}} \\ \qquad\qquad + \max\left(0, \dfrac{\left(v_0\left(t_0^{\text{e}}\right)\right)^2 - \left(v_5\left(t_0^{\text{e}}\right)\right)^2}{2g\mu}\right) \\ d_{n,0}^{\text{lat}}\left(t_0^{\text{e}}\right) = d_{n,5}^{\text{lat}}\left(t_0^{\text{e}}\right) \\ v_{n,0}^{\text{lon}}\left(t_0^{\text{e}}\right) = v_{n,5}^{\text{lon}}\left(t_0\right) \\ v_{n,0}^{\text{lat}}\left(t_0^{\text{e}}\right) = 0 \end{cases} \tag{21}$$

where μ is the EV sliding resistance coefficient.

Additionally, to address the collision risk posed by the unpredictable movements of surrounding vehicles, this paper introduces constraints for suspending the LC process. If these constraints are satisfied, the LC process will be terminated, and the vehicle will adopt the preceding vehicle in the original lane as the target vehicle. The constraints for terminating the LC process are defined as follows:

$$\left| d_1^{\text{lat}} - d_0^{\text{lat}} \right| < l_w \Rightarrow d_1^{\text{lon}} - d_0^{\text{lon}} \geq C + \frac{\left(v_0^{\text{lon}}\right)^2 - \left(v_1^{\text{lon}}\right)^2}{2g\mu} \tag{22a}$$

$$\left| d_5^{\text{lat}} - d_0^{\text{lat}} \right| < l_w \Rightarrow d_5^{\text{lon}} - d_0^{\text{lon}} \geq C + \frac{\left(v_0^{\text{lon}}\right)^2 - \left(v_5^{\text{lon}}\right)^2}{2g\mu} \tag{22b}$$

where l_w is the vehicle's width.

D. Strategy solving algorithm

The potential LC process can be defined by varying the LC start position, acceleration duration, uniform motion duration, deceleration duration, angular velocity of the front wheel angle, and the duration of angle increase, constant angle, and angle decrease. By applying the constraints and objective function, the optimal LC trajectory is selected from all feasible trajectories. The corresponding EV powertrain and steering system control variables are then determined based on the pre-processed acceleration and deceleration phases. The strategy-solving algorithm is outlined in Algorithm 1.

VI. Case Study and Discussion

The two-stage LC strategy proposed in this paper comprises two main components: LCD, which replicates the driver's LC habits, and LCI, which leverages the EV's dynamic characteristics. The paper first examines the sensitivities of both LCD and LCI, including the effects of factor number and LCI on LCD, as well as the influence of trajectory objectives and LCD on LCI. Subsequently, to verify the robustness of the proposed strategy, and highlight the essential differences between EVs and fuel vehicles in the LC process, its performance under varying states of charge and environmental temperatures is analyzed. In order to better compare the performance of the proposed strategies, this paper compares the proposed LCD

Algorithm 1 Two-stage LC strategy solving algorithm

Parameter initialization: Initialize $t = 0$, and initialize the state variable values $d_1^{\text{lon}}(t), d_3^{\text{lon}}(t), d_5^{\text{lon}}(t)$ for LCD; the initial state variable values $\beta(t), \psi(t), v_0(t), SOC(t)$ for LCI model; initialize the time step Δt and time horizon $t_{\max}$.
while $t < t_{\max}$ **do**
Step 1 (LCD). Judge the LCD according to Eq. (17): if $\mathrm{L}_n^* = 1$, go to **Step 2**; otherwise, go to **Step 7**.
Step 2 (LC ending point). Determine the place and velocity at the end of LC according to Eq. (21).
Step 3 (Feasible LCI). Feasible LCI trajectory generation with the following sub-steps.
Step 3.1. Discretize the variables to be optimized with Eq. (19);
Step 3.2. Calculate the acceleration and deceleration processes used in the LC process according to Eqs. (7)- (10);
Step 3.3. Use dynamic programming algorithms to obtain the feasible LC trajectories according to Eqs. (4)-(6), (13)-(15) and the corresponding performance in Eq. (18).
Step 4 (Trajectory selection). Select the optimal LC trajectory from all feasible trajectories and determine the corresponding optimized variables.
Step 5 (Condition Check). Determine whether to execute optimized control variables for the powertrain and steering systems according to Eq. (22).
Step 6 (Update). Update the state variables and time step based on the optimized variables executed at time t according to Eqs. (4)-(10).
Step 7 (Time increasing). $t \leftarrow t + \Delta t$
end while

TABLE V
THE PARAMETERS INVOLVED IN THE CASE STUDIES

Parameter	Value	Parameter	Value
$k_f(N/rad)$	-62618	$k_r(N/rad)$	-110185
$l_f(m)$	1.463	$l_r(m)$	1.585
$I_z(kg*m^2)$	3885	$r_{\text{whe}}(m)$	0.307
$t^{\text{lc,max}}(s)$	10	$k^{\delta,\max}(rad/s)$	$\pi/6$
$v_{n,0}^{\text{lc,min}}(m/s)$	0	$v_{n,0}^{\text{lc,max}}(m/s)$	45
$\delta^{f,\min}(rad)$	$-\pi/4$	$\delta^{f,\max}(rad)$	$\pi/4$
μ	0.7		

model with the MOBIL model [51], [52], and compares the proposed LCI model with the polynomial trajectory [53], [54].

The parameters involved in the case studies are shown in the Tab. V. Additionally, To explore the performance of strategies from a holistic perspective, this paper constructs the cases according to the extracted motion differences before and after LC from the dataset. Meanwhile, in order to better illustrate the specific situation of the strategy, the 12th set of LC trajectory data is employed to illustrate the strategy's performance. The trajectories of the 12th LC vehicle and its surrounding six vehicles are depicted in Fig. 12.

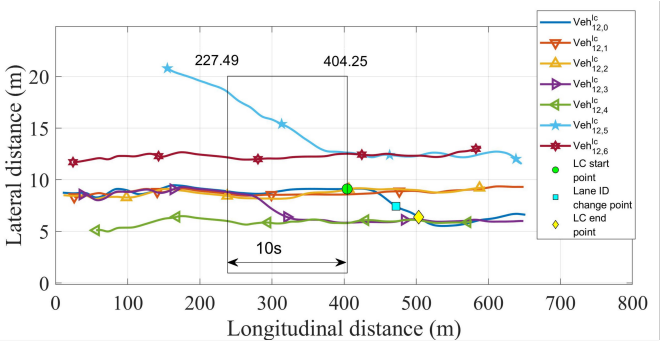

Fig. 12. The trajectories of the 12th LC vehicle and its surrounding 6 vehicles

A. LCD sensitivity analysis

1) Number of considering factors: The number of factors considered is critical in constructing the LCD model, as different factor selections result in varied model properties. In order to comprehensively explore the performance of the proposed LCD model, this paper incorporates all LC data from the dataset into the model and obtains corresponding LCD data, as shown in Fig. **??**. The normalized LCD prediction values considering 2, 4, and 28 influencing factors and the MOBIL model are presented. Due to the selection of data 10s before the LC start point, the vehicle changed lanes at the 10th second. It can be seen from this that with the increase of consideration factors, there are increasingly obvious maximum points in the first 10 seconds, while the MOBIL model does not exhibit this property. This conclusion can be well supported by the average LCD prediction value (see Fig. 14), as the LCD models considering 4 and 28 influencing factors have the peak values around 1.6s. That means driver's executed LC decision requires an obvious LC opportunity to prompt, and can be a strong proof of accuracy shown in Fig. 5.

TABLE VI
THE MEANS OF PREDICTED VALUES AND 95% CONFIDENCE INTERVALS

Factor number	Data before LC		LC start point	
	Mean	Interval	Mean	Interval
2	0.53	[0.531, 0.532]	0.55	[0.546, 0.559]
4	0.53	[0.530, 0.533]	0.60	[0.581, 0.611]
28	0.53	[0.530, 0.533]	0.63	[0.614, 0.648]

The effectiveness of the LC key point identification is further demonstrated in Table VI, which presents statistical graphs of the LCD model's predicted values before LC and at the LC start point, along with the corresponding mean predicted values and 95% confidence intervals. There is a significant difference between the predicted values before LC and at the LC start point. The average predicted value before

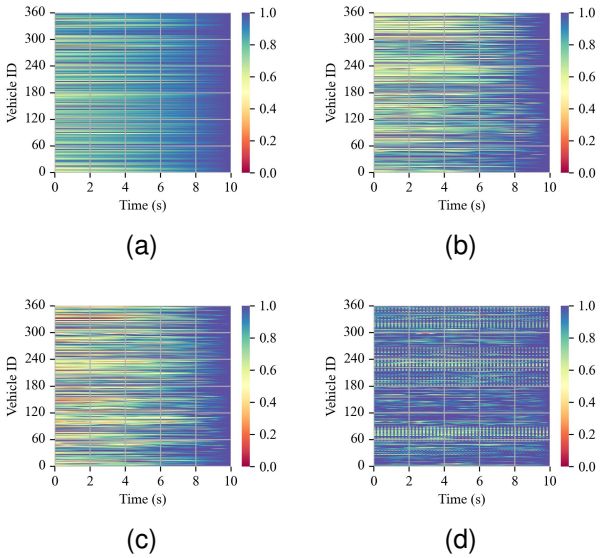

Fig. 13. The normalized predicted value of LCD models in the dataset. (a) 2 factors; (b) 4 factors; (c) 28 factors; (d) MOBIL.

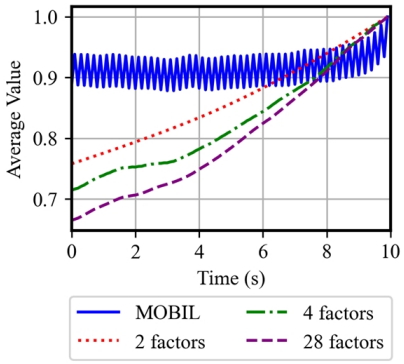

Fig. 14. The average normalized predicted value of LCD models in the dataset.

LC is 0.53, while at the LC start point, the average predicted values for LCD models considering 2, 4, and 28 factors are 0.55, 0.60, and 0.63, respectively, with no overlap in their 95% confidence intervals. This demonstrates that the proposed method for identifying LC key points effectively recognizes the LC start point.

After completing the overall statistical analysis, this paper takes the 12th vehicle as an example to analyze the specific changes in LCD model values. As illustrated in Fig. 15, the predicted value proportions of LCD models considering 2, 4, and 28 factors are shown using the 12th LC vehicle as an example, which was randomly selected for this study, as well as the MOBIL model. The sensitivity of the LCD models to vehicle motion information increases with the number of factors considered. When only 2 factors are considered, the change in predicted values is relatively smooth, and the model accurately identifies the LC starting point, where the predicted value reaches its maximum. However, with 4 factors, slight fluctuations occur, with three instances where the predicted value exceeds that at the LC starting point before the LC.

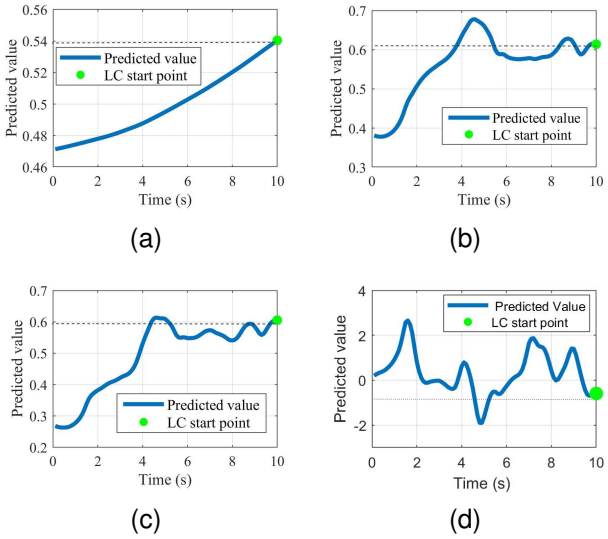

Fig. 15. The predicted value of LCD models for the 12th LC vehicle.(a) 2 factors; (b) 4 factors; (c) 28 factors; (d) MOBIL.

When 28 factors are considered, the model becomes extremely sensitive to changes in the vehicle's motion state. But the MOBIL model failes to leverage its advantages in interaction and dynamic changes, due to the lack of interaction between vehicles.

2) The impacts of LCI on LCD: The impact of the LCI stage on the LCD stage is primarily reflected in the influence of longitudinal space on the LCD predicted value. A larger longitudinal space at the LC start point allows more LC trajectories for vehicles to execute. However, differences in longitudinal space result in varying LCD predicted values, indicating changes in the consistency between the LCD model and driving habits. The positive correlation between longitudinal LC space and LCD prediction values is widely present in the models constructed considering different influencing factors. However, the MOBIL model cannot reflect this because it mainly focuses on the acceleration gain after switching.

As shown in Fig.16, the map displays the longitudinal position of the front vehicle in the original lane, the longitudinal position of the front vehicle in the target lane, and the LCD predicted values considering 2, 4, and 28 influencing factors. It is evident that, regardless of the number of factors considered, the predicted value decreases with the increase in the longitudinal position of the front vehicle in the original lane and increases with the increase in the longitudinal position of the front vehicle in the target lane.

Furthermore, Fig.17 presents a map showing the longitudinal position of the LC vehicle, the longitudinal position of the front vehicle in the original lane, the longitudinal position of the front vehicle in the target lane, and the predicted value considering 28 influencing factors. From this, it can be observed that the predicted value is independent of the longitudinal position of the LC vehicle, negatively correlated with the longitudinal position of the front vehicle in the original lane, and positively correlated with the longitudinal position of the front vehicle in the target lane. Therefore, the

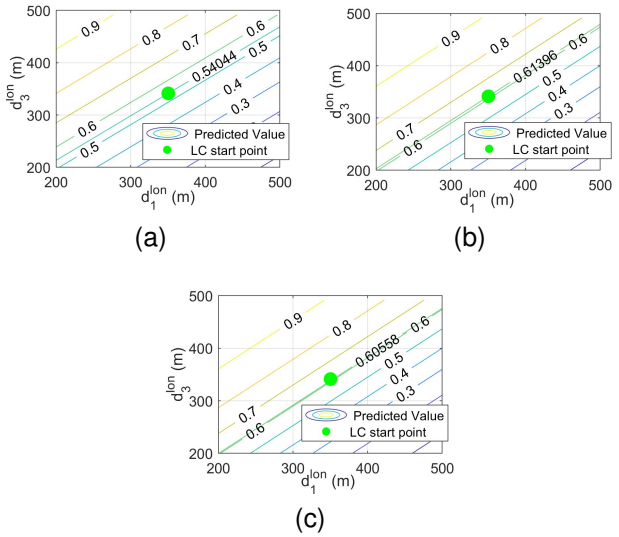

Fig. 16. The LCD predicted value sensitivity to LC longitudinal space. (a) 2 factors; (b) 4 factors; (c) 28 factors.

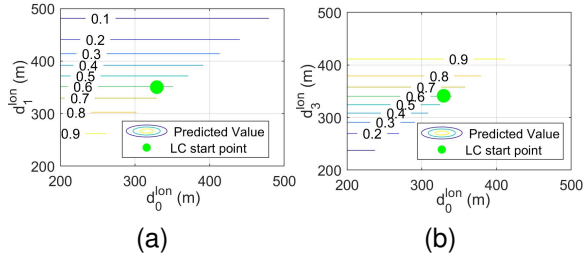

Fig. 17. The LCD predicted value sensitivity to preceding longitudinal space under 28 factors. (a) Original lane; (b) Target lane.

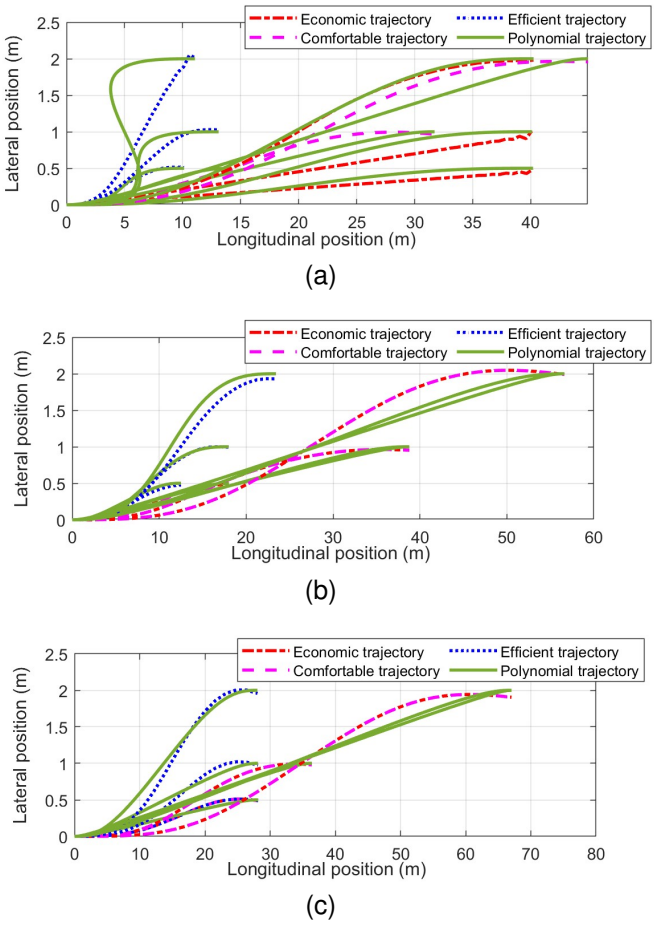

Fig. 18. Comparison of trajectories for achieving specific lateral displacement under different velocity changes. (a) 5 m/s to 5.5 m/s; (b) 10 m/s to 11 m/s; (c) 15 m/s to 16.5 m/s.

greater the longitudinal position difference between the front vehicle in the target lane and the front vehicle in the original lane, the higher the LCD predicted value, and the stronger the driver's willingness to change lanes.

B. LCI Sensitivity Analysis

1) Multi-objective LCI trajectory: The LCI stage optimization considers consistency, economy, comfort, and efficiency in the LC process. It is important to note that when only considering consistency, the proposed LCI optimization strategy cannot obtain a complete trajectory and can only determine the LC starting point. Therefore, this paper sets the weight coefficients of the objective function to [0,1,0,0], [0,0,1,0], and [0,0,0,1], respectively. Additionally, the SOC and environmental temperature are set to 70% and 27°C, respectively.

During the LCI phase, drivers achieve lateral displacement changes through driving operation, resulting in significant differences before and after implementation. By comparing the dataset before and after this stage, it can be found that the average lateral displacement is 1.7m, the average velocity change is 0.9m/s, and the average starting velocity is 11.2m/s. Therefore, in order to explore the sensitivity of the proposed strategy, this paper divides cases based on the differences before and after this stage in the dataset, and combines them with fifth degree polynomial trajectories to explore the universal performance of LCI. The Fig, **??** shows the economic, comfortable, efficient, and fifth degree polynomial trajectory of LC vehicles performing different lateral displacement changes under different motion states. At this time, the starting velociyt of the LC vehicle is set to 5m/s, 10m/s, and 15m/s, respectively, with corresponding velocity changes of 0.5m/s, 1m/s, and 1.5m/s, and lateral displacements of 0.5m, 1m, and 2m, respectively. As the starting velocity increases, the economic trajectory and comfort trajectory gradually overlap, while the efficient trajectory is always limited by the velocity changes adopted by the strategy, which fails to fully utilize the dynamic characteristics of EVs to achieve fast steering. Polynomial trajectory can achieve the same trajectory motion effect well, but it requires sacrificing additional motion, especially the efficient trajectory at low velocity, resulting in reverse situations.

Uses data from the 12th LC vehicle to obtain the corresponding optimized trajectory.And, the performance related to economic, comfortable, and efficient can be seen in Tab. VII. The dynamics of EV, including position, acceleration, and wheel angle, in the multi-objective LCI trajectory are presented in Fig. 19. From Fig. 19(a), it can be observed that the required longitudinal spaces for the economical, comfort-

TABLE VII
THE LCI PERFORMANCE CONSIDERING ECONOMIC, COMFORTABLE, AND EFFICIENT

Trajectory type	Angular velocity (rad/s)	SOC consumption (%/m)	LC time (s)
Economic	0.105	0.000678	4.41
Comfortable	0.0176	0.000686	4.21
Efficient	0.314	0.000949	1.71

able, and efficient trajectories are 3.1%, 16.2%, and 203.8% larger than those for the original trajectory, respectively. The economical and comfortable trajectories almost overlap, making full use of the longitudinal space to ensure a smooth LC trajectory, while the efficient trajectory completes the LC process within a shorter longitudinal displacement. From Figs. 19(b) and (c), it is evident that the optimized trajectories have selected the same economical acceleration, and the changes in acceleration and wheel angle follow the preset patterns. The angular velocities for the economical, comfortable, and efficient trajectories are 0.105 rad/s, 0.0176 rad/s, and 0.314 rad/s, respectively. The comfortable trajectory demonstrates 83.2% and 94.4% better performance than the economical and efficient trajectories, respectively. The completion times for lateral displacement in the efficient, comfortable, economical, and original trajectories are 1.71 s, 4.21 s, 4.41 s, and 5.7 s, respectively. As a result, the required lane change times for the economical, comfortable, and efficient trajectories are 70.0%, 26.1%, and 22.6% shorter than those for the original trajectory, respectively. Thus, the proposed optimization strategy achieves significant performance improvements in both space and time.

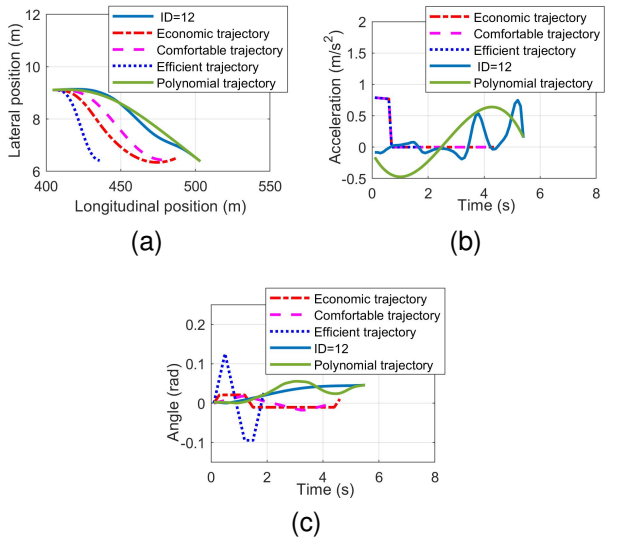

Fig. 19. EV dynamics in multi-objective LCI trajectory for the 12th LC vehicle. (a) Position; (b) Acceleration; (c) Wheel angle.

In Fig. 20, the states of the LC EV powertrain in the multi-objective LCI trajectory are illustrated. Under simulation conditions of 70% SOC and an environmental temperature of 27°C, the operating state of the EV powertrain is closely related to the power required by the LC vehicle. Based on

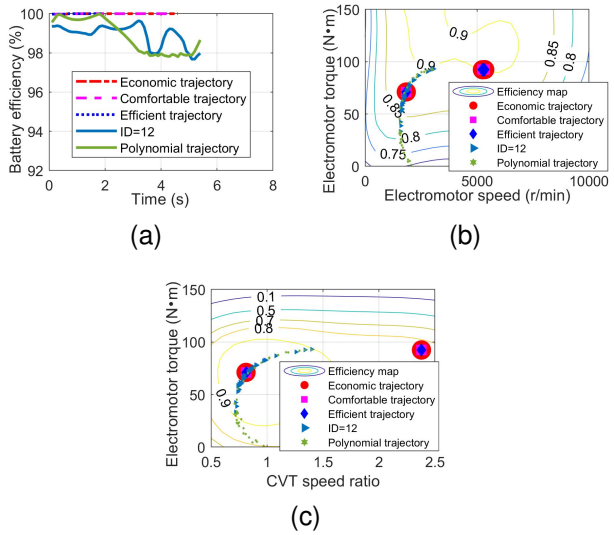

Fig. 20. EV powertrain states in multi-objective LCI trajectory under different SOCs for the 12th LC vehicle. (a) Battery; (b) Electromotor; (c) CVT.

Fig. 20, Fig. 19(a), and Eq. (7), it can be observed that when the LC vehicle accelerates, the powertrain needs to output higher power, which leads to decreased efficiency in the battery, electromotor, and continuously variable transmission. After acceleration, the LC EV transitions to a uniform motion state, where the required power decreases and the powertrain reaches a more optimal operating state. Furthermore, the SOC changes per meter for the economic, comfortable, and efficient trajectories are 0.000678%/m, 0.000686%/m, and 0.000949%/m, respectively. The energy consumption of the economic trajectory is 28.6% lower than that of the efficient trajectory.

2) The impacts of LCD on LCI: The impact of the LCD stage on the LCI stage is primarily reflected in how the available longitudinal space for LC influences the LCI process.

TABLE VIII
THE TRAJECTORY PERFORMANCE UNDER VARIOUS LIMITED LONGITUDINAL SPACES

Limited longitudinal space (m)	Economic trajectory SOC change (%)	Comfortable trajectory angular velocity (rad/s)	Efficient trajectory LC time (s)
35	0.000925	0.227	1.71
60	0.00075	0.0670	1.71
85	0.000678	0.0176	1.71
110	0.000678	0.0176	1.71

Fig. 21 and Tab. VIII illustrate the trajectory differences under various limited longitudinal spaces, specifically the longitudinal position difference between the LC EV and the vehicle ahead in the target lane. In Fig. 21(a), it can be observed that as the longitudinal space increases, the energy consumption of the economic trajectory decreases, although this trend diminishes progressively. By increasing the longitudinal space, the SOC change per meter can be reduced from 0.000925%/m to 0.000678%/m, representing a 26.7% decrease.

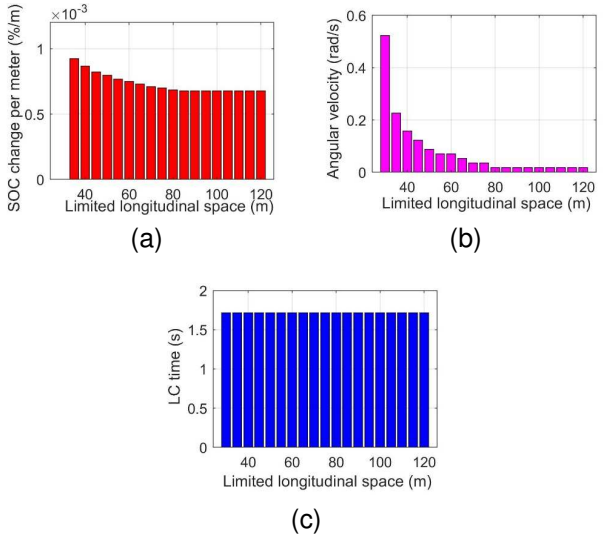

Fig. 21. Multi-objective LCI performance under different maximum longitudinal space. (a) Economic; (b) Comfortable; (c) Efficient.

Similarly, in Fig. 21(b), the performance of the comfort trajectory follows a pattern comparable to the economic trajectory. Increasing the longitudinal space reduces the steering wheel angular velocity of the comfortable trajectory from 0.524 rad/s to 0.0176 rad/s, a significant reduction of 96.6%. However, it is important to note that the performance improvement of the comfort trajectory is constrained by the degree of dispersion and the maximum value of the steering wheel angular velocity. From Figs. 21(c) and 19(a), it is evident that there is a minimum longitudinal space required for efficient trajectories, which is determined by the maximum angular velocity of the steering wheel, as indicated in Eq.14.

C. The robustness of the LC strategy

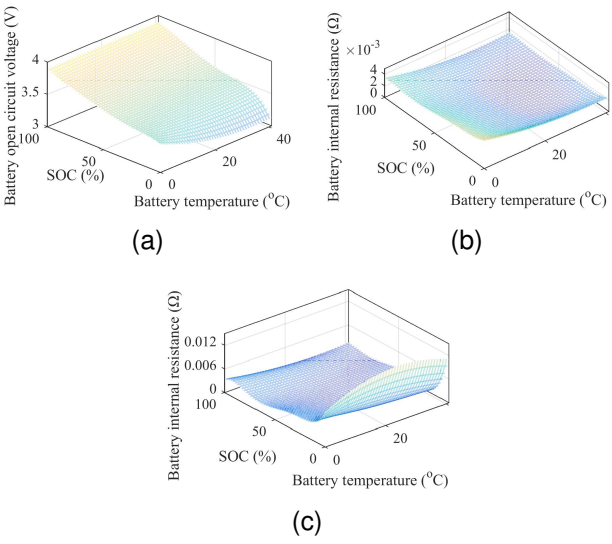

Fig. 22. EV battery performance fitting results. (a) Battery voltage; (b) Charge internal resistance; (c) Discharge internal resistance.

Unlike the relatively stable performance of fuel vehicles, the performance of EVs is closely related to the SOC and environmental temperature, as described in Eq.(22). In this equation, the internal resistance and voltage of the battery are functions of SOC and environmental temperature. And, the fitting curves of battery voltage, discharge resistance, and charging internal resistance are shown in the Fig.22, according to Eqs. (9b), (9c), and (9f). Therefore, the superior performance of the proposed strategy across a wide range of SOCs and environmental temperatures under realistic conditions ensures its adaptability.

This paper constructs a simulation environment based on data from the 12th LC vehicle to explore the adaptability of the proposed strategy using economic trajectories. First, the robustness to different SOCs is examined by setting the environmental temperature to 27°C and testing SOCs at 70%, 30%, and 10%, respectively. In addition, to study robustness to varying environmental temperatures, the SOC is fixed at 70%, and the temperatures are set to -27°C, -17°C, 27°C, and 37°C, respectively.

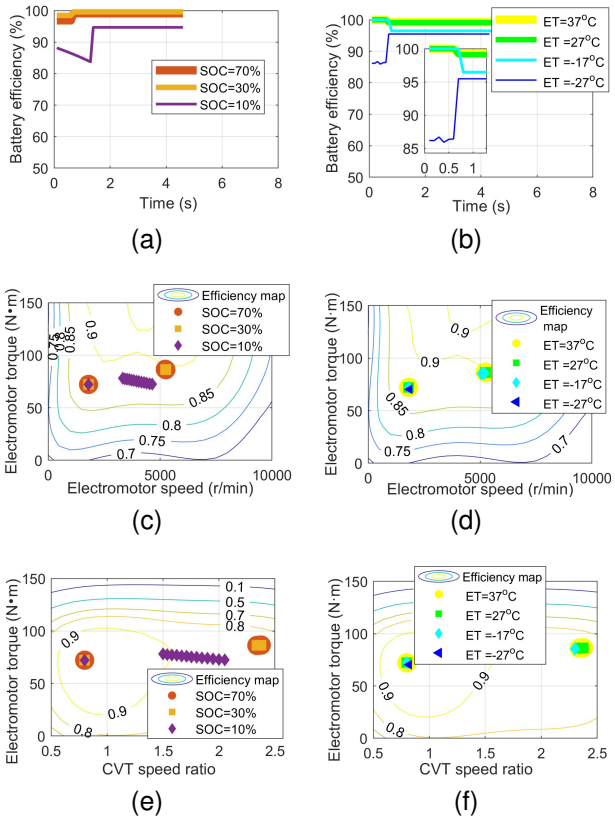

Fig. 23. EV powertrain states in economical driving strategy under different SOCs and environment temperatures. (a) and (b) are the battery states; (c) and (d) are the electromotor states; (e) and (f) are the CVT states.

The performance differences of the proposed strategies under different SOCs and environmental temperatures can be examined through battery efficiency, electromotor efficiency, and CVT efficiency, as shown in Fig.23. By combining Eq. (7) with Fig. 8, it is evident that the influence of SOC and environmental temperature on the proposed strategy is primarily due to variations in battery internal resistance and battery voltage under different conditions. Regarding SOC, as SOC

decreases from 70% to 10%, the internal resistance and voltage of the battery initially remain stable, followed by an increase in internal resistance and a decrease in voltage, leading to a reduction in battery efficiency. Consequently, the operating status of the electromotor and CVT is not only dependent on EV velocity but is also strongly influenced by lower SOC levels. When SOC drops to 10%, the operating states of the battery, electromotor, and CVT continuously adjust to compensate for the decreasing battery efficiency during acceleration. However, during uniform motion, the power required by the EV is minimal and constant, resulting in stable powertrain operation. In contrast, when the environmental temperature drops from 37°C to -17°C, the changes in battery internal resistance and voltage are relatively minor, allowing the battery efficiency to remain high. Therefore, the operating status of the electromotor and CVT in this case is primarily related to the EV velocity. It is worth noting that when the temperature drops to -27, the efficiency of the battery rapidly decreases from 96.2% to 86.3% during the acceleration process This is because during the acceleration process, the battery needs to provide a higher current to complete the acceleration process. When the temperature drops to a certain value, as shown in the Fig. 22, as the temperature decreases, the voltage of the battery decreases and the resistance increases, resulting in a decrease in efficiency at low temperatures.

Thus, it can be inferred that the fundamental difference between EVs and fuel vehicles during LC strategies is the difference in velocity variation performance caused by powertrain. The powertrain of an electric vehicle includes a battery and an electromotor. The battery is used to convert chemical and electrical energy, while the electromotor is used to convert electrical and mechanical energy. During this process, the voltage and resistance of the battery are highly sensitive to environmental temperature and SOC (as shown in the Fig.**??**), resulting in complex spatiotemporal characteristics of the EV dynamic characteristic. The powetrain of fuel vehicles mainly includes internal combustion engines, which are used to achieve the conversion of chemical energy and machinery. This process is relatively smooth and generally not affected by the external environment (except for atmospheric pressure differences caused by large altitude differences). Therefore, the LC strategy for EVs needs to be closely linked to the state of the EV (e.g., SOC) and driving conditions (e.g., environment temperature). However, considering the initial velocity and stable operating range of battery performance, the performance difference between EVs and fuel vehicles during LC is positively correlated with the magnitude of velocity changes. In this context, the proposed strategy can not only utilize autonomous driving technology to achieve differentiated LC processes for EVs, but also dynamically introduce LC optimization variables for EVs based on autonomous driving computing power, to assist in the electrification and intelligent development of transportation systems.

VII. Conclusion

With the rapid advancement of vehicle automation and electrification, it is important to use intelligent assisted driving to enhance the EV driving efficiency; while the assisted driving strategy should ensure the driver feels comfortable. This paper presents a two-stage LC strategy for optimizing both LCD and LCI considering driving habit and EV dynamics. First, a set of trajectory data of the LC vehicle and its six surrounding vehicles were analyzed to identify key LC points, calculate the correlation between LCD and vehicle motion information, and construct a logit-based LCD model. Next, the paper examines EV displacement changes considering dynamic characteristics, explores the effects of LCI on the powertrain and steering system, and proposes a trajectory generation method based on different LC starting position. Then, the overall LC strategy framework was developed, which integrately optimizes the LCD and LCI stages based on driving habits and vehicle dynamics.

In the numerical tests, we conduct some sensitivity analyses on the LCD model with different factor combinations and on the LCI model with different parameters. We also analyze the driving performance with the proposed LCI model with different objective functions. The results indicate that optimizing the LC starting point by adjusting longitudinal space can synergistically improve both the LCD and LCI stages, which verifies the effectiveness of the proposed strategy. In addition, the results also indicate that the proposed strategy is robust in different scenarios with different initial SOCs and environmental temperatures.

The existing research correlates the driving habits and the EV dynamic characteristics, and proposes autonomous LC strategies that meet differentiated objectives. However, existing research has overlooked the dynamic evolution characteristics of driving habits and the optimization requirements for specific scenarios. Therefore, future work will expand the forms of optimization variables to adapt to the dynamic evolution process of driving habits, and explore implantable LC strategies for specific and realistic driving scenarios.

Acknowledgement

This study is funded by the National Natural Science Foundation of China (72201149, 72288101), the Natural Science Foundation of Shandong Province (ZR2024QE314), and the Fundamental Research Funds for the Central Universities (202413022).

References

[1] H. Singh and A. Kathuria, "Analyzing driver behavior under naturalistic driving conditions: A review," Accident Analysis & Prevention, vol. 150, p. 105908, 2021.

[2] M. N. Azadani and A. Boukerche, "Driving behavior analysis guidelines for intelligent transportation systems," IEEE transactions on intelligent transportation systems, vol. 23, no. 7, pp. 6027–6045, 2021.

[3] Z. Zheng, "Recent developments and research needs in modeling lane changing," Transportation research part B: methodological, vol. 60, pp. 16–32, 2014.

[4] S. Singh, "Critical reasons for crashes investigated in the national motor vehicle crash causation survey," Tech. Rep., 2015.

[5] F. W. Siebert, M. Oehl, F. Bersch, and H.-R. Pfister, "The exact determination of subjective risk and comfort thresholds in car following," Transportation research part F: traffic psychology and behaviour, vol. 46, pp. 1–13, 2017.

[6] P. G. Gipps, "A model for the structure of lane-changing decisions," Transportation Research Part B: Methodological, vol. 20, no. 5, pp. 403–414, 1986.

[7] Q. I. Yang and H. N. Koutsopoulos, "A microscopic traffic simulator for evaluation of dynamic traffic management systems," Transportation Research Part C: Emerging Technologies, vol. 4, no. 3, pp. 113–129, 1996.

[8] C.-J. Jin, V. L. Knoop, D. Li, L.-Y. Meng, and H. Wang, "Discretionary lane-changing behavior: Empirical validation for one realistic rule-based model," Transportmetrica A: transport science, vol. 15, no. 2, pp. 244–262, 2019.

[9] D.-F. Xie, Z.-Z. Fang, B. Jia, and Z. He, "A data-driven lane-changing model based on deep learning," Transportation research part C: emerging technologies, vol. 106, pp. 41–60, 2019.

[10] W. Wang, T. Qie, C. Yang, W. Liu, C. Xiang, and K. Huang, "An intelligent lane-changing behavior prediction and decision-making strategy for an autonomous vehicle," IEEE transactions on industrial electronics, vol. 69, no. 3, pp. 2927–2937, 2021.

[11] Y. Ali, Z. Zheng, M. M. Haque, M. Yildirimoglu, and S. Washington, "Clacd: A complete lane-changing decision modeling framework for the connected and traditional environments," Transportation Research Part C: Emerging Technologies, vol. 128, p. 103162, 2021.

[12] P. I. Richards, "Shock waves on the highway," Operations research, vol. 4, no. 1, pp. 42–51, 1956.

[13] J. A. Laval and C. F. Daganzo, "Lane-changing in traffic streams," Transportation Research Part B: Methodological, vol. 40, no. 3, pp. 251–264, 2006.

[14] A. K. Das and U. Chattaraj, "Cellular automata model for lane changing activity," International Journal of Intelligent Transportation Systems Research, vol. 20, no. 2, pp. 446–455, 2022.

[15] G. Park, S. Lee, S. Jin, and S. Kwak, "Integrated modeling and analysis of dynamics for electric vehicle powertrains," Expert Systems with Applications, vol. 41, no. 5, pp. 2595–2607, 2014.

[16] M. Amrhein and P. T. Krein, "Dynamic simulation for analysis of hybrid electric vehicle system and subsystem interactions, including power electronics," IEEE transactions on vehicular technology, vol. 54, no. 3, pp. 825–836, 2005.

[17] S. Manzetti and F. Mariasiu, "Electric vehicle battery technologies: From present state to future systems," Renewable and Sustainable Energy Reviews, vol. 51, pp. 1004–1012, 2015.

[18] Z. Dai and J. Ye, "Computer statistical and big data analysis on the comparisons between traditional engine, electromotor, and hybrid systems," Highlights in Science, Engineering and Technology, vol. 29, pp. 119–130, 2023.

[19] J. Ruan, P. Walker, and N. Zhang, "A comparative study energy consumption and costs of battery electric vehicle transmissions," Applied energy, vol. 165, pp. 119–134, 2016.

[20] Z. Zhang, K. Chau, and Z. Wang, "Analysis and stabilization of chaos in the electric-vehicle steering system," IEEE transactions on vehicular technology, vol. 62, no. 1, pp. 118–126, 2012.

[21] A. Broggi, M. Buzzoni, S. Debattisti, P. Grisleri, M. C. Laghi, P. Medici, and P. Versari, "Extensive tests of autonomous driving technologies," IEEE Transactions on Intelligent Transportation Systems, vol. 14, no. 3, pp. 1403–1415, 2013.

[22] S. Gupta, A. K. Tripathi, and V. Parameswaran, "Attention transfer-based deep distilled architecture for 6g driven-smart vehicle transportation system," IEEE Transactions on Intelligent Transportation Systems, 2024.

[23] A. Gasparetto, P. Boscariol, A. Lanzutti, and R. Vidoni, "Path planning and trajectory planning algorithms: A general overview," Motion and operation planning of robotic systems: Background and practical approaches, pp. 3–27, 2015.

[24] I. Mir, F. Gul, S. Mir, M. A. Khan, N. Saeed, L. Abualigah, B. Abuhaija, and A. H. Gandomi, "A survey of trajectory planning techniques for autonomous systems," Electronics, vol. 11, no. 18, p. 2801, 2022.

[25] G. Qing, Z. Zheng, and X. Yue, "Path-planning of automated guided vehicle based on improved dijkstra algorithm," in 2017 29th Chinese control and decision conference (CCDC). IEEE, 2017, pp. 7138–7143.

[26] Y. Shi, Q. Li, S. Bu, J. Yang, and L. Zhu, "Research on intelligent vehicle path planning based on rapidly-exploring random tree," Mathematical Problems in Engineering, vol. 2020, no. 1, p. 5910503, 2020.

[27] H. Marzbani, H. Khayyam, Đ. V. Quoc, and R. N. Jazar, "Autonomous vehicles: Autodriver algorithm and vehicle dynamics," IEEE Transactions on Vehicular Technology, vol. 68, no. 4, pp. 3201–3211, 2019.

[28] L. G. Véras, F. L. Medeiros, and L. N. Guimaraes, "Rapidly exploring random tree* with a sampling method based on sukharev grids and convex vertices of safety hulls of obstacles," International Journal of Advanced Robotic Systems, vol. 16, no. 1, p. 1729881419825941, 2019.

[29] K. Kawabata, L. Ma, J. Xue, C. Zhu, and N. Zheng, "A path generation for automated vehicle based on bezier curve and via-points," Robotics and Autonomous Systems, vol. 74, pp. 243–252, 2015.

[30] T. Maekawa, T. Noda, S. Tamura, T. Ozaki, and K.-i. Machida, "Curvature continuous path generation for autonomous vehicle using b-spline curves," Computer-Aided Design, vol. 42, no. 4, pp. 350–359, 2010.

[31] R. Chai, A. Tsourdos, A. Savvaris, S. Chai, and Y. Xia, "Solving constrained trajectory planning problems using biased particle swarm optimization," IEEE Transactions on Aerospace and Electronic Systems, vol. 57, no. 3, pp. 1685–1701, 2021.

[32] W. Lim, S. Lee, M. Sunwoo, and K. Jo, "Hierarchical trajectory planning of an autonomous car based on the integration of a sampling and an optimization method," IEEE Transactions on Intelligent Transportation Systems, vol. 19, no. 2, pp. 613–626, 2018.

[33] Y. Zha, J. Deng, Y. Qiu, K. Zhang, and Y. Wang, "A survey of intelligent driving vehicle trajectory tracking based on vehicle dynamics," SAE International journal of vehicle dynamics, stability, and NVH, vol. 7, no. 10-07-02-0014, pp. 221–248, 2023.

[34] A. P. Aguiar and J. P. Hespanha, "Trajectory-tracking and path-following of underactuated autonomous vehicles with parametric modeling uncertainty," IEEE transactions on automatic control, vol. 52, no. 8, pp. 1362–1379, 2007.

[35] D. Chu, H. Li, C. Zhao, and T. Zhou, "Trajectory tracking of autonomous vehicle based on model predictive control with pid feedback," IEEE Transactions on Intelligent Transportation Systems, vol. 24, no. 2, pp. 2239–2250, 2022.

[36] C.-L. Hwang, C.-C. Yang, and J. Y. Hung, "Path tracking of an autonomous ground vehicle with different payloads by hierarchical improved fuzzy dynamic sliding-mode control," IEEE Transactions on Fuzzy Systems, vol. 26, no. 2, pp. 899–914, 2017.

[37] B. Coifman and L. Li, "A critical evaluation of the next generation simulation (ngsim) vehicle trajectory dataset," Transportation Research Part B: Methodological, vol. 105, pp. 362–377, 2017.

[38] V. Punzo, M. T. Borzacchiello, and B. Ciuffo, "On the assessment of vehicle trajectory data accuracy and application to the next generation simulation (ngsim) program data," Transportation Research Part C: Emerging Technologies, vol. 19, no. 6, pp. 1243–1262, 2011.

[39] Q. Liu, S. Xu, C. Lu, H. Yao, and H. Chen, "Early recognition of driving intention for lane change based on recurrent hidden semi-markov model," IEEE transactions on vehicular technology, vol. 69, no. 10, pp. 10 545–10 557, 2020.

[40] H. Woo, Y. Ji, H. Kono, Y. Tamura, Y. Kuroda, T. Sugano, Y. Yamamoto, A. Yamashita, and H. Asama, "Lane-change detection based on vehicle-trajectory prediction," IEEE Robotics and Automation Letters, vol. 2, no. 2, pp. 1109–1116, 2017.

[41] H. Qi, C. Chen, X. Hu, and J. Zhang, "Online inference of lane changing events for connected and automated vehicle applications with analytical logistic diffusion stochastic differential equation," Transportation Research Part C: Emerging Technologies, vol. 144, p. 103874, 2022.

[42] Z. Ma, S. Shi, X. Liu, B. Zhang, and N. Lin, "Linearization and robust stability analysis of two degree-of-freedom vehicle dynamics model," in 2023 7th CAA International Conference on Vehicular Control and Intelligence (CVCI). IEEE, 2023, pp. 1–6.

[43] W. Chen, D. Tan, H. Wang, and X. G. Wang Jiaen, "A class of driver directional control model based on trajectory prediction," Journal of Mechanical Engineering, vol. 52, no. 14, pp. 106–105, 2016.

[44] C. Liu and Y. Liu, "Energy management strategy for plug-in hybrid electric vehicles based on driving condition recognition: a review," Electronics, vol. 11, no. 3, p. 342, 2022.

[45] M. Coleman, C. Zhu, C. Lee, and W. Hurley, "A combined soc estimation method under varied ambient temperature for a lead-acid battery," in Twentieth Annual IEEE Applied Power Electronics Conference and Exposition, 2005. APEC 2005., vol. 2. IEEE, 2005, pp. 991–997.

[46] H. Vu and D. Shin, "Scheduled pre-heating of li-ion battery packs for balanced temperature and state-of-charge distribution," Energies, vol. 13, no. 9, p. 2212, 2020.

[47] P. Liao, T.-Q. Tang, R. Liu, and H.-J. Huang, "An eco-driving strategy for electric vehicle based on the powertrain," Applied Energy, vol. 302, p. 117583, 2021.

[48] J. Ruan, P. D. Walker, J. Wu, N. Zhang, and B. Zhang, "Development of continuously variable transmission and multi-speed dual-clutch transmission for pure electric vehicle," Advances in Mechanical Engineering, vol. 10, no. 2, p. 1687814018758223, 2018.

[49] S. Akehurst, N. Vaughan, D. Parker, and D. Simner, "Modelling of loss mechanisms in a pushing metal v-belt continuously variable transmission. part 1: torque losses due to band friction," Proceedings of the

Institution of Mechanical Engineers, Part D: Journal of Automobile Engineering, vol. 218, no. 11, pp. 1269–1281, 2004.
[50] T.-Q. Tang, P. Liao, H. Ou, and J. Zhang, "A fuel-optimal driving strategy for a single vehicle with cvt," Physica A: Statistical Mechanics and its Applications, vol. 505, pp. 114–123, 2018.
[51] A. Kesting, M. Treiber, and D. Helbing, "General lane-changing model mobil for car-following models," Transportation Research Record Journal of the Transportation Research Board, vol. 1999, pp. 86–94, 2007.
[52] D. Helbing and A. Greiner, "Modeling and simulation of multi-lane traffic flow," Physical Review E Statistical Physics Plasmas Fluids Related Interdisciplinary Topics, vol. 55, no. 5, pp. 5498–5508, 1998.
[53] M. Werling, J. Ziegler, S. Kammel, and S. Thrun, "Optimal trajectory generation for dynamic street scenarios in a frenet frame," in Robotics and Automation (ICRA), 2010 IEEE International Conference on, 2010.
[54] Perez, Joshue, Milanes, Vicente, Gonzalez, David, Nashashibi, and Fawzi, "A review of motion planning techniques for automated vehicles," IEEE Transactions on Intelligent Transportation Systems, 2016.

Peng Liao received the B.S. and the Ph.D. degrees from Beihang University, Beijing, China.

He is currently a Lecturer with the College of Engineering, Ocean University of China. His research interest includes the driving strategy and the powertrain optimization.

Tao Wang received the B.S. and the Ph.D. degrees from Beihang University, Beijing, China. He was Postdoctoral Fellow in ETS Lab, School of Vehicle and Mobility, Tsinghua University, Beijing, China.

He is currently an Associate professor with the School of Automotive and Transportation Engineering, Hefei University of Technology. His research interests include the travel choice modeling, traffic flow theory and planning the intelligent traffic system.

Tie-Qiao Tang received the B.S. and M.S. degrees from Hunan Normal University, Changsha, China, and the Ph.D. degree from Beihang University, Beijing, China.

He is currently a Professor with the School of Transportation Science and Engineering, Beihang University, China. His research areas include traffic flow theory, traffic safety, pedestrian traffic, and air traffic.

Ronghui Liu received the B.S. degree from Peking University, China, and the Ph.D. degree from Cam bridge University, U.K.

She is currently a Professor with the Institute for Transport Studies, University of Leeds. Her main research interests include developing traffic microsimulation models to analyze the dynamic and complex travel behavior and interactions in transport networks.